A RECONSTRUCTION OF AEROTHERMAL ENVIRONMENT AND THERMAL PROTECTION SYSTEM RESPONSE OF THE MARS SCIENCE LABORATORY ENTRY VEHICLE

Deepak Bose,[*] Todd White,[†] Milad Mahzari,[§] and Karl Edquist[‡]

An initial assessment and reconstruction of Mars Science Laboratory (MSL) entry aerothermal environment and thermal protection system (TPS) response is performed using the on-board instrumentation suite called MSL Entry, Descent, and Landing Instrumentation (MEDLI). The analysis is performed using the current best estimated trajectory. The MEDLI suite in part provides in-depth temperature measurements at seven locations on the heatshield. The temperature data show the occurrence of boundary layer transition to turbulence on the leeside forebody of the entry vehicle. The data also suggest that the TPS recession is lower than nominal model predictions using diffusion limited surface oxidation. The model predictions of temperatures show an underprediction in the stagnation and apex regions, and an overprediction in the leeside region. An estimate of time-varying aeroheating using an inverse reconstruction technique is also presented. The reconstructed aeroheating is sensitive to the choice of a recession model.

INTRODUCTION

NASA's Mars Science Laboratory (MSL), which entered the atmosphere of Mars on August 5th, 2012 and landed the 900 kg *Curiosity* rover, represented a significant advancement in planetary entry, descent, and landing capability.[1] With an entry mass of 3200 kg and a 4.5 m diameter heatshield (see Fig. 1), MSL was the heaviest and the largest Mars entry vehicle. In addition, the entry vehicle flew a guided hypersonic trajectory at a nominal angle of attack of 16-deg generating a lift-over-drag ratio of 0.24. The moderately high entry speed of 5.9 km/s, coupled with high ballistic coefficient, and a large running length on the forebody, was likely to cause turbulent heating augmentation. To protect the vehicle against expected high heating, a new tiled thermal protection system made with Phenolic-Impregnated Carbon Ablator (PICA) was used.[2] A constant thickness TPS was designed to withstand heating as high as 226 W/cm^2 and heat loads of up to 6400 J/cm^2.[3,4]

The selection and sizing of the TPS of an entry vehicle uses predictive models in computational fluid dynamics (CFD) and ablative material response codes. The CFD code provides the aerothermal load on the vehicle as it flies along a hypersonic trajectory and the material response code computes the in-depth temperatures and material decomposition. These predictive tools are developed using physics based models that are validated in small-scale ground tests performed in wind tunnels, shock tubes, and arc heated facilities. While ground test facilities are essential for validation of these models, they are not adequate substitutes for actual flight environment. The validation of aerothermal and material response codes for Mars entry has

*Aerospace Engineer, NASA Ames Research Center, Moffett Field, CA 94035, USA
†Research Scientist, ERC, Inc., Moffett Field, CA 94035, USA
§Graduate Research Assistant, Georgia Institute of Technology, Atlanta, GA 30332, USA
‡Aerospace Engineer, NASA Langley Research Center, Hampton, VA 23681, USA

thus far relied solely on ground test due to a lack of flight data. As a result, the predictions of the models are left with large uncertainties. Table 1 shows a summary of major uncertainties and design margins applied in MSL heatshield design. These uncertainties are substantial and are a result of phenomena that are not adequately addressed and validated in ground test facilities. A combined impact of these uncertainties is estimated to lead to more 40% extra forebody TPS thickness on MSL heatshield relative to zero-margin thickness.[4] While additional ground based validation could lead to small incremental improvements in these uncertainties, flight validation is required to achieve a substantial improvement. A flight validated aerothermal and TPS response model would not only lead to mass efficient designs, but also positively impact development of new systems and technologies by relaxing testing and qualification requirements that are currently based on similarly margined loads. With the above considerations in mind, the MSL heatshield was instrumented to acquire critical flight data for aerodynamics, aerothermodynamics, and thermal protection system response.[5,6] The instrumentation suite is called Mars Science Laboratory Entry, Descent, and Landing Instrumentation (MEDLI).

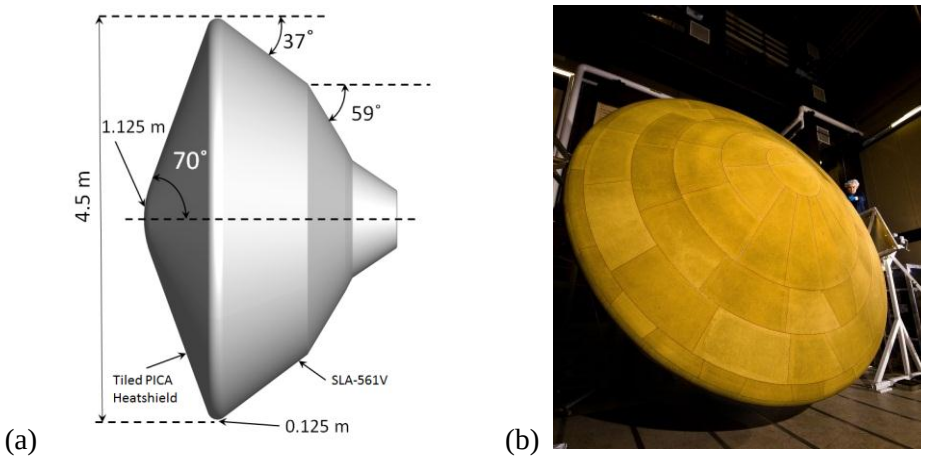

Figure 1. (a) MSL entry vehicle and (b) MSL heatshield made with PICA titles (photo credit: Lockheed Martin Space Systems)

Table 1. Summary of Model Uncertainties and Margins used for TPS design

Source	Uncertainty/Margin	Reference
Supercatalytic Heating	20%-30%	Ref. 7
Stagnation Point Heating	50%	Ref. 3
Turbulent Roughness Augmentation	20%-30%	Ref. 3
Boundary Layer Transition	Fully Turbulent	Ref. 3
Thermal Margin	45-60F	Ref. 4
TPS Recession	150%	Ref. 4

The MEDLI suite consists of 7 pressure transducers, 24 thermocouples, and 6 ablation sensors. It successfully acquired and returned surface pressure, in-depth temperatures, and material decomposition characteristics at various locations on the heatshield. The MEDLI suite on MSL represents the most extensively instrumented Mars entry heatshield. Heatshield instrumentation in past Mars entry missions has been minimal. The Viking entry vehicle included two backshell thermocouples, one of which malfunctioned prior to peak heating.[8] Mars Pathfinder

had nine in-depth thermocouples in the TPS and many of them failed to return useable data.[9,10] In addition to extensive instrumentation, MSL's unique entry, large aeroshell, and high ballistic coefficient, provided an opportunity to measure turbulent heating augmentation that was not expected in past Mars entries.

The MEDLI dataset is currently being used to reconstruct vehicle aerodynamics, aerothermal environment, and TPS response during entry. This paper presents an assessment of the thermal data received, performs some initial comparisons of in-depth temperatures with model predictions, and provides preliminary estimates of the aerothermal environment.

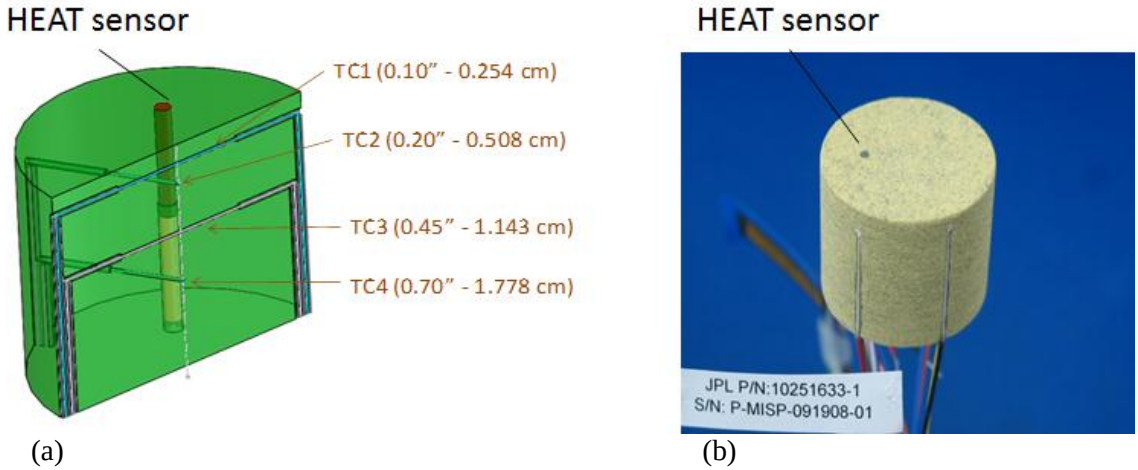

Figure 2. (a) Schematic of a MISP plug with four Type-K thermocouples and a HEAT sensor (b) MISP plug made with PICA

Table 2 X-Ray depths of as-installed thermocouples in each MISP and plug locations on the heatshield. See Fig. 3 for X-Y coordinate system.

	TC Depths				Plug Layout on Heatshield	
Plug	**TC1**	**TC2**	**TC3**	**TC4**	**Y**	**X**
	mm	*mm*	*mm*	*mm*	*m*	*m*
MISP1	2.65	5.09	11.49	17.87	-0.798	0.000
MISP2	2.68	5.16	11.57	17.77	1.957	-0.447
MISP3	2.61	4.91	11.59	17.60	1.957	0.442
MISP4	2.47	5.39	11.32	17.94	-1.270	0.002
MISP5	2.53	4.86			0.227	0.000
MISP6	2.73	5.15	11.67	17.66	1.240	-0.001
MISP7	2.39	4.89			0.519	0.000

MEDLI INSTRUMENTATION LAYOUT AND OPERATION

The MEDLI instrumentation suite is comprised of two classes of sensors: one for surface pressure measurements called Mars Entry Atmospheric Data System (MEADS) and a second

suite of instrumentation for thermal performance (temperature and charring) of the heatshield called the MEDLI Integrated Sensor Plug (MISP). Reference 11 describes the use of MEADS pressure data for reconstruction of vehicle aerodynamics and atmospheric properties. This paper and Refs. 12 and 13 present the initial analysis of MISP data for reconstruction of aerothermal environments and TPS response. The details of MEDLI hardware and environment testing are discussed in Refs. 6 and 14

Table 3 MEADS pressure port locations on the heatshield. See Fig. 3 for X-Y coordinate system.

Port	Y *m*	X *m*
MEADS 1	-1.403	0.000
MEADS 2	-0.991	0.000
MEADS 3	-0.310	0.000
MEADS 4	0.000	0.000
MEADS 5	0.310	0.000
MEADS 6	0.000	0.991
MEADS 7	0.000	-0.991

The MISP instrumentation is embedded in 1.3" diameter and 1.14" deep PICA cylindrical plugs. Each MISP plug contained four Type-K (chromel-alumel) thermocouples with 0.012" wire diameter at nominal depths of 0.1, 0.2, 0.45. and 0.7 inch (0.254, 0.508, 1.143, and 1.778 cm) from the initial surface as shown in Figure 2(a) and (b). The measured depths of as-installed plugs using X-Ray images are given in Table 2. The top thermocouples are expected to be more responsive to changes in the surface heating conditions, while the deeper thermocouples are expected to measure in-depth thermal response as heat is conducted through the thickness of the recessing and pyrolyzing material. In addition to the thermocouples, an ablation sensor, called the HEAT sensor (Hollow aErothermal Ablation and Temperature)[15] is also installed through the thickness as shown in Fig. 2. A total of seven MISP plugs are installed on the heatshield. The layout of the plugs is shown in Fig. 3(a) and their locations on the heatshield are given in Table 2. Each plug is installed on the heatshield using the RTV-560 silicone-elastomer bonding agent. The plugs are numbered as follows. MISP 1 & 4 are installed in the stagnation region of the forebody while MISP 5 & 7 are embedded in the apex region to capture maximum laminar heating. MISP 2,3, & 6 are located in the leeside forebody to capture turbulent heating levels, as this region is expected to experience maximum heat flux. The plugs are arranged along or near the line of symmetry to capture the development and progression of the boundary layer transition front along the center streamline. MISP 2 & 3 are installed slightly away from the centerline to assess asymmetric heating due to any side-slip angle. No plugs are installed in the backshell of the vehicle. The MEADS pressure ports are installed on the windside forebody of the vehicle as shown in Fig. 3(b). The layout is designed to enable a reconstruction of vehicle attitude and freestream dynamic pressure during hypersonic flight. The locations of MEADS ports are given in Table 3. No MEADS ports are installed on the backshell of the vehicle.

The MEDLI system, which includes MEADS and MISP instrumentation, and the System Support Electronics box, was turned on five hours before entry on August 5th, 2012. The cruise temperatures in the plugs were found to be within -115˚C to -78˚C. Approximately ten minutes before entry MEDLI began to acquire data. A subset of the critical MEDLI data was transmitted real time during EDL including tones to indicate incremental progression of events. The full MEDLI dataset was stored in the rover for transmission to earth at a later time. The data sampling

rate varied from 1-8Hz depending on the sensor. The full dataset was successfully received on earth a few days after landing.

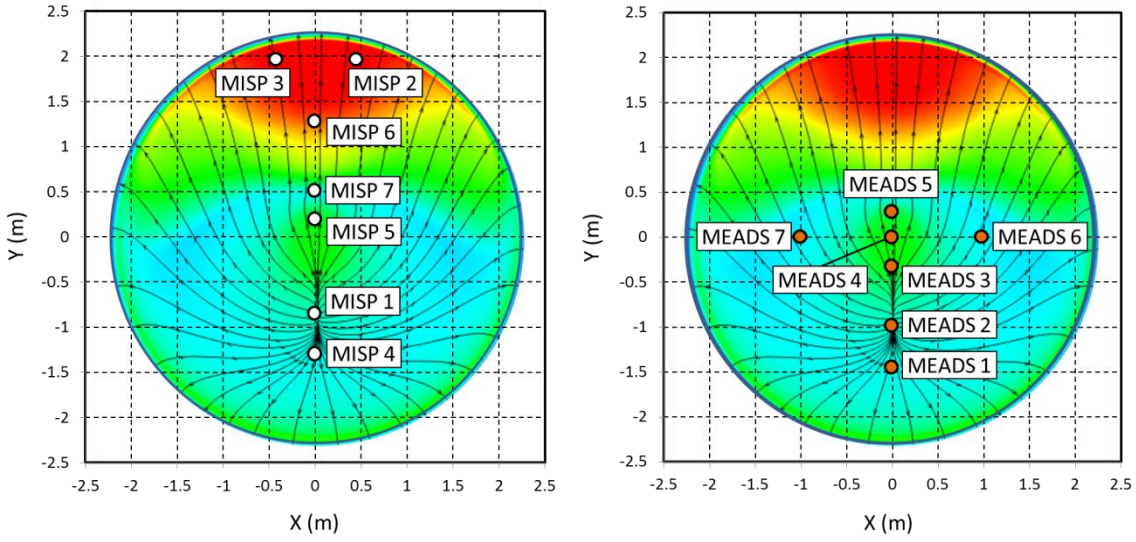

(a) (b)

Figure 3 (a) MISP plug layout (b) MEADS port locations on MSL heatshield

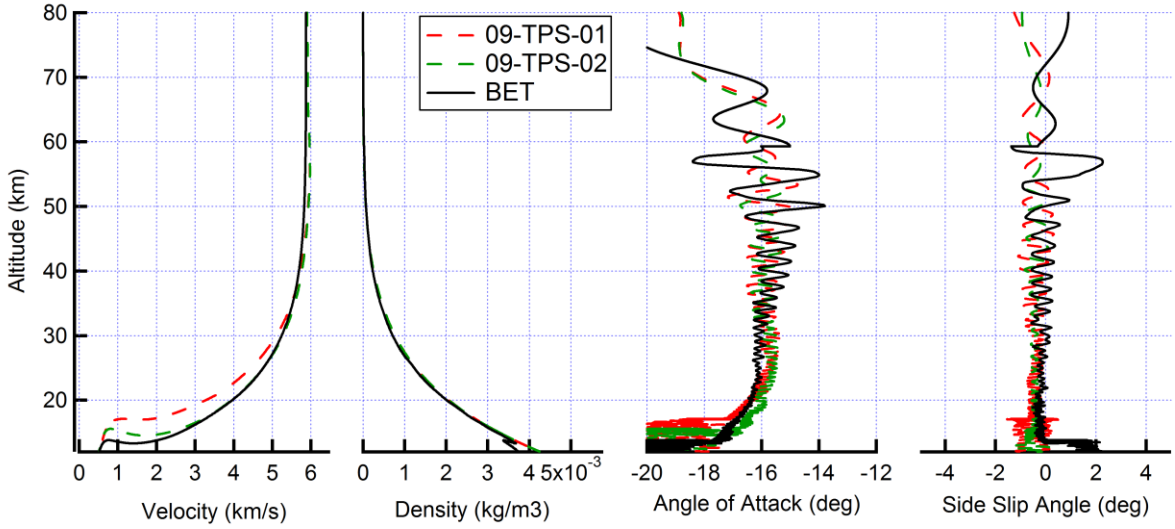

Figure 4 Design and Best Estimated Trajectories

MSL DESIGN AND BEST ESTIMATED TRAJECTORIES

The aerothermal environments for MSL TPS design were based on two trajectories: a steep trajectory (09-TPS-02, flight path angle=-15.5 deg) and a shallow trajectory (09-TPS-01, entry flight path angle=-14 deg). The 09-TPS-02 trajectory was used to calculate the maximum heat flux, shear stress, and pressure whereas the 09-TPS-01 trajectory was used to size the TPS as it had a higher heat load. The design trajectories used the allocated entry mass (3308 kg) and a high entry velocity in the launch arrival window (5.9 km/s), both of which make the aerothermodynamic environments more severe. The best estimated trajectory (BET) was obtained

using on-board inertial measurements and MEADS pressure data to estimate dynamic pressure, atmospheric density and temperature, and vehicle attributes.[11] A comparison of the BET and the 09-TPS design trajectories are shown in Fig. 4. The BET entry mass and velocity are lower than design trajectories, which would tend to produce lower heating. The BET entry flight path angle, however, is steeper than the design trajectories, which tends to increase maximum heating. The angle of attack and side-slip angles are also shown in Fig. 4. The side-slip angle is less than 2-deg in the hypersonic portion of the flight. The analysis in this work will assume no side-slip to take advantage of the pitch plane symmetry in CFD simulations.

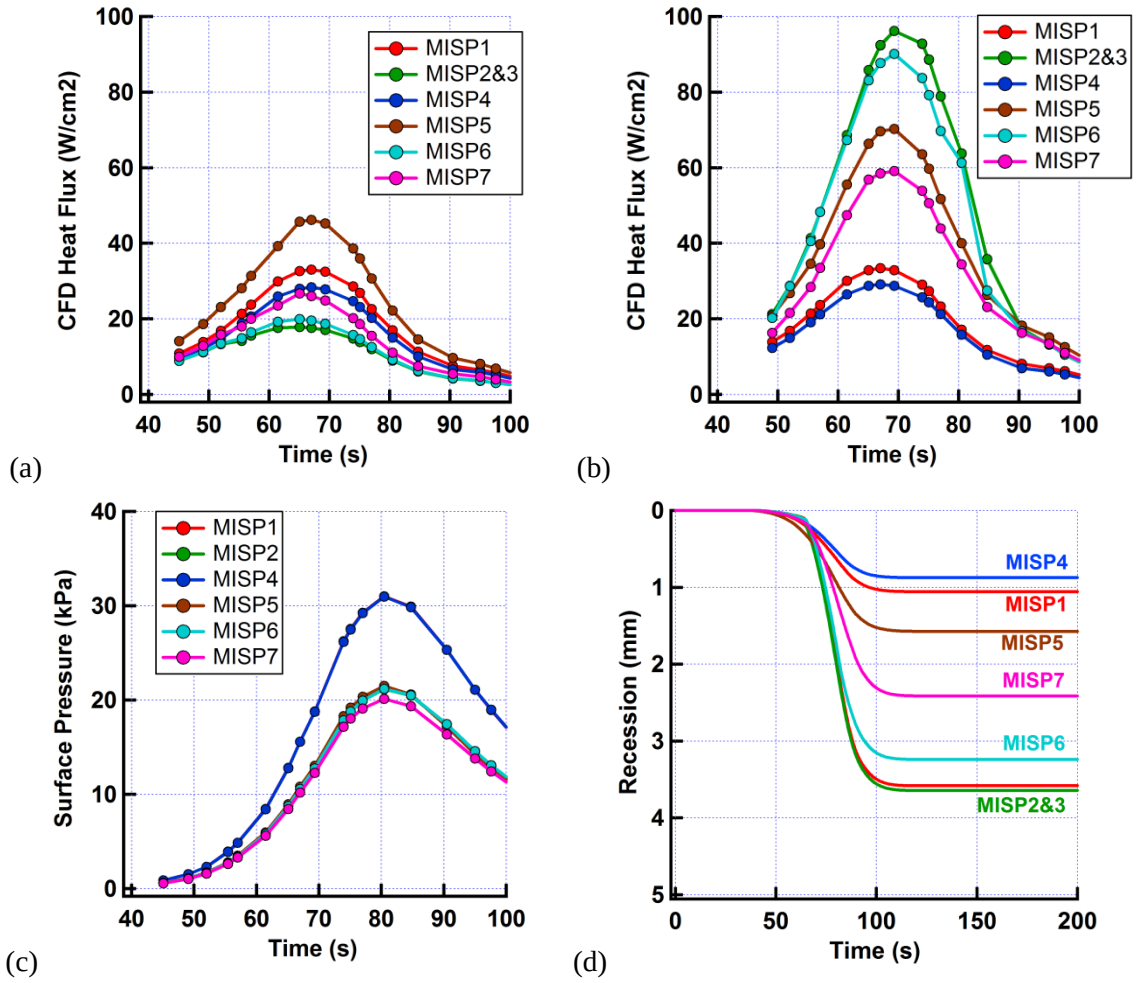

Figure 5 CFD predicted (a) laminar and (b) turbulent heat flux, (c) pressure, and (d) predicted recession from FIAT on seven MISP plug locations during MSL entry.

MODELING TOOLS AND NOMINAL PREDICTIONS

CFD and Material Response Codes

For the model predictions presented here we use two CFD codes, Data-Parallel Line Relaxation (DPLR),[16] and Langley Aerothermodynamic Upwind Relaxation Algorithm (LAURA),[17] and one ablator material response code called Fully Implicit Ablation and Thermal Response Program (FIAT).[18] DPLR and LAURA are parallel, structured non-equilibrium CFD code developed at NASA Ames and Langley Research Centers respectively. The codes solve

compressible Reynolds Averaged Navier-Stokes equations for chemically reacting fluid flow with heat transfer.

FIAT is an implicit ablation and thermal response program for simulation of one-dimensional transient thermal energy transport in a multilayer stack of isotropic materials that can ablate from a front surface and decompose in-depth. FIAT is developed by scientists at the NASA Ames Research Center and is a standard tool in the aerospace industry today for the thermal sizing and analysis of spacecraft heatshields. The equations solved in the FIAT code are the internal energy balance, internal decomposition, internal mass balance and surface energy balance equations. The surface energy balance is solved using pre-calculated surface blowing rate, B′ tables derived under the assumption of thermochemical equilibrium at the surface. FIAT version 2.6 and PICA material model version 3.3[19] are used in this work.

Nominal Aerothermal Predictions on Best Estimated Trajectory

The nominal aerothermal and surface recession predictions are made for the BET using DPLR and FIAT codes. For nominal predictions, the flow around the heatshield is modeled as thermochemical non-equilibrium flow, using the Mitcheltree and Gnoffo[20] 8-species (CO_2, CO, N_2, O_2, NO, C, N, and O) Mars model. The Mars atmosphere is modeled as 97% CO_2 and 3% N_2 by mass. The TPS surface is modeled as an unblown, no-slip, radiative equilibrium wall with constant emissivity ($\varepsilon = 0.89$) and the Mitcheltree and Gnoffo surface catalycity model. Species diffusion is modeled using self-consistent effective binary diffusion. Turbulent flow is simulated with the Baldwin-Lomax algebraic model. CFD calculations are performed along the entry trajectory, at 2-5 second intervals. Surface properties for material response simulations are extracted from the CFD solutions at each MISP location. These quantities are then fitted in time with tight monotonic cubic splines, and provided as inputs to the FIAT material response code at quarter-second intervals. The CFD generated aerothermal environment imposed on material response modeling is switched from laminar to turbulent heating at specific times when boundary layer transition is observed in flight data. The boundary layer transition times observed in flight data will be discussed in a later section. For recession prediction FIAT assumes equilibrium chemistry and diffusion limited oxidation. Figure 5 shows nominal laminar heat flux, turbulent heat flux, pressure, and surface recession predictions at the seven MISP plugs during entry. Table 4 compares nominal CFD heating environments on BET to the margined environments used for TPS design on 09-TPS trajectories.

Table 4 Aerothermal design and BET nominal environments at MISP locations

Plug	Design Heat Flux W/cm^2	BET Nominal Heat Flux W/cm^2
MISP 1	63	33
MISP 2	219	96
MISP 3	219	96
MISP 4	57	29
MISP 5	119	70
MISP 6	212	90
MISP 7	129	59

MISP FLIGHT DATA AND INITIAL OBSERVATIONS

MISP Data

The complete MEDLI dataset stored in the rover was received a few days subsequent to the successful landing of *Curiosity*. Channels of raw voltages and currents were converted into thermocouple temperatures and HEAT sensor resistances. All 24 MISP temperatures and 6 HEAT sensor resistances as a function time were received. Four thermocouple traces were obtained for each MISP plug, except plugs 5 and 7 which did not have the two deepest thermocouples (TC3 and TC4) wired due to number of channel limitations. The as-received MISP temperatures are shown in Fig. 6. All thermocouples returned data successfully, and the traces appear to be virtually noise free. The data from the HEAT sensors, however, showed unusual behavior during the heat pulse. The HEAT sensor data are still being assessed for quality and will be presented in future papers. The pressure data from the MEADS pressure transducers were also returned successfully, and will be used for comparisons with CFD predictions.

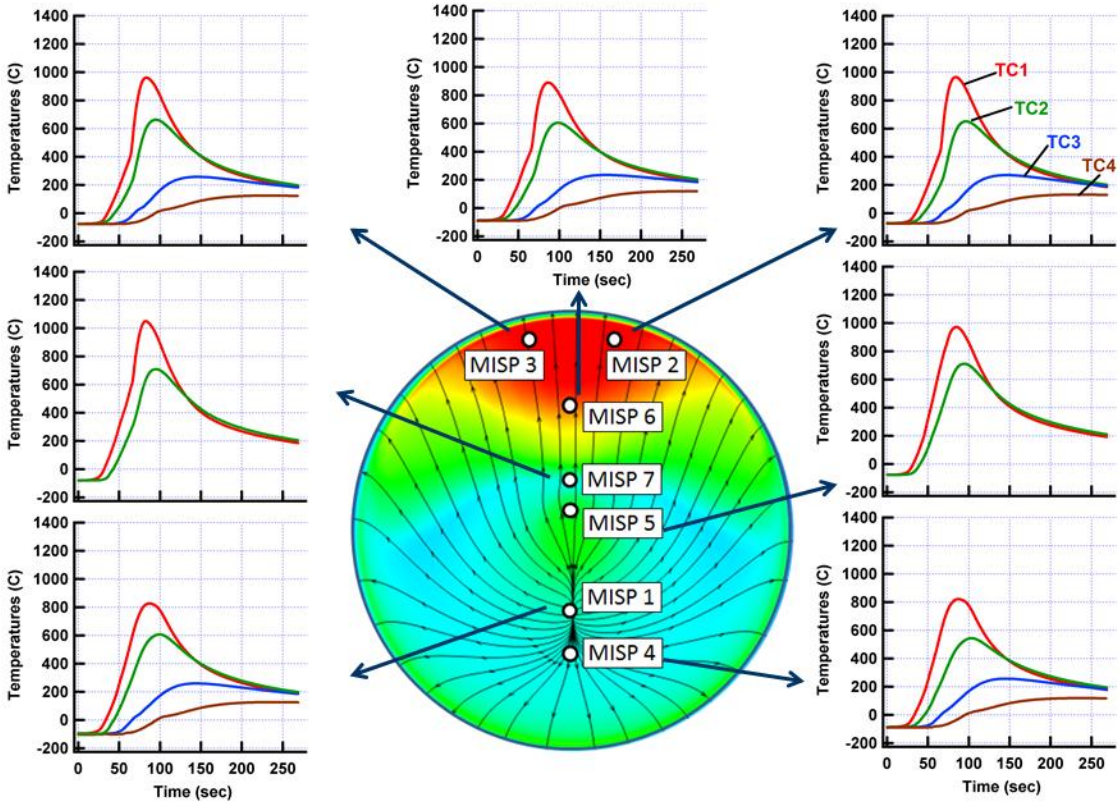

Figure 6 MISP thermocouple data obtained during MSL entry. TC1, TC2, TC3, and TC4 represent readings of thermocouples at depths shown in Table 2.

Surface Recession

One key observation that is made from the flight data is the absence of any near surface thermocouple burnout. This indicates that the TPS did not recede past any of the shallow thermocouples [nominally 0.1-inch (2.54 mm) below the unablated surface]. While it is possible that a thermocouple would survive in the event the TPS recedes beyond its depth and it is exposed to the boundary layer flow, it is unlikely to be the case. A thermocouple exposed in the

boundary layer would measure very high temperatures since boundary layer temperatures rise very rapidly away from the surface. It is therefore concluded that the TPS did not recess more than 0.1-inch (2.54 mm), which is lower than the nominal predictions shown in Fig. 5(d). The nominal predictions show that the TPS recession front moves deeper than the near surface thermocouple depths at MISP 2,3,6, and 7. In MISP7, while the recession front does not reach the nominal near surface thermocouple depth of 0.1-inch, it crosses the as-installed depth of 0.094-inch (see Table 2). The systematic overprediction of recession is perhaps to be expected as it is evident in comparisons with arc jet test data at low heat fluxes in stagnation conditions.[21] It is hypothesized that kinetic rate-limiting surface oxidation is responsible for a low recession relative to FIAT predictions which assumes a faster diffusion limited oxidation. At this time no kinetic rate-limited recession model for PICA exists that is sufficiently validated for use in TPS design.

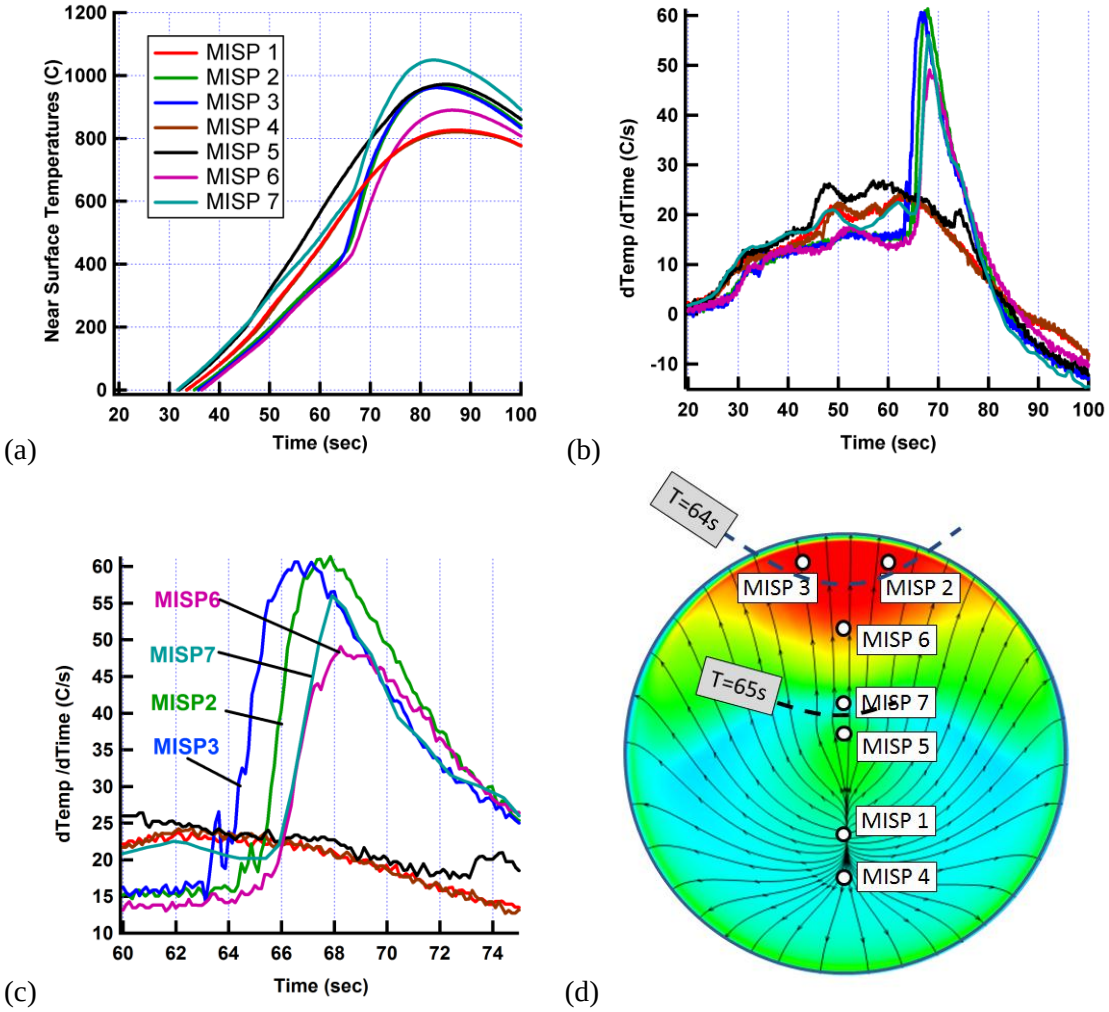

Figure 7 (a) Top thermocouple [0.1 inch (2.54 mm) deep] data from each MISP plug, (b) temperature-time slope of top thermocouple data, (c) magnified temperature-time slope of top thermocouple data, and (d) notional transition front on the aeroshell.

Boundary Layer Transition

Boundary layer transition from laminar to turbulent flow is a phenomenon of great practical importance due to its significant impact on aeroheating and shear stress. The prediction of

boundary layer transition, however, is extremely challenging as it is triggered by a variety of poorly understood factors such as flow disturbance (noise), surface roughness, pyrolysis gas blowing, etc. For TPS design the prediction of boundary layer transition is usually made by using simple criteria imposed on momentum thickness or roughness Reynolds numbers. These criteria are developed based on ground tests and their validity in flight environment is unknown. MISP data provides the first opportunity to assess predictive capability of these techniques for Mars entry. It should be noted that the sizing of the TPS was performed using the most conservative assumption of a fully turbulent aerothermal environment due to poor confidence in existing transition predictive capability. A significant reduction in aeroheating load is realizable on a large area of the heatshield if a reliable boundary layer transition prediction model is available.

The transition of boundary layer from laminar to turbulent flow causes a sudden rise in aeroheating which can be identified by a corresponding sudden change in the slope of the temperature traces. Such a change of slope is apparent in the MISP thermocouple traces in Fig. 6 at the leeside locations, confirming that the leeside of the vehicle did experience a transition to turbulence. The onset of turbulence before peak heating is apparent on four leeside plugs: MISP 2, 3, 6, & 7 as seen in Fig. 7. The windside plugs (MISP 1 and 4) do not show onset of turbulence, which is consistent with expectations. MISP 5, close to the apex, shows a late boundary layer transition at ~73 sec. The transition to turbulence is most obvious in the near surface thermocouples due to their proximity to the surface; the signal is progressively muted in deeper thermocouples. Figure 7 (a) shows the near surface thermocouple traces from all seven plugs. A more obvious demonstration of boundary layer transition is seen in Fig. 7(b) and (c) where temporal slopes of temperature traces are simultaneously plotted for every plug. It is seen that transition first begins at MISP3, and a second later is followed by MISP2, and within roughly another second the transition front reaches upstream to MISP7, as schematically shown in Fig. 7 (d).

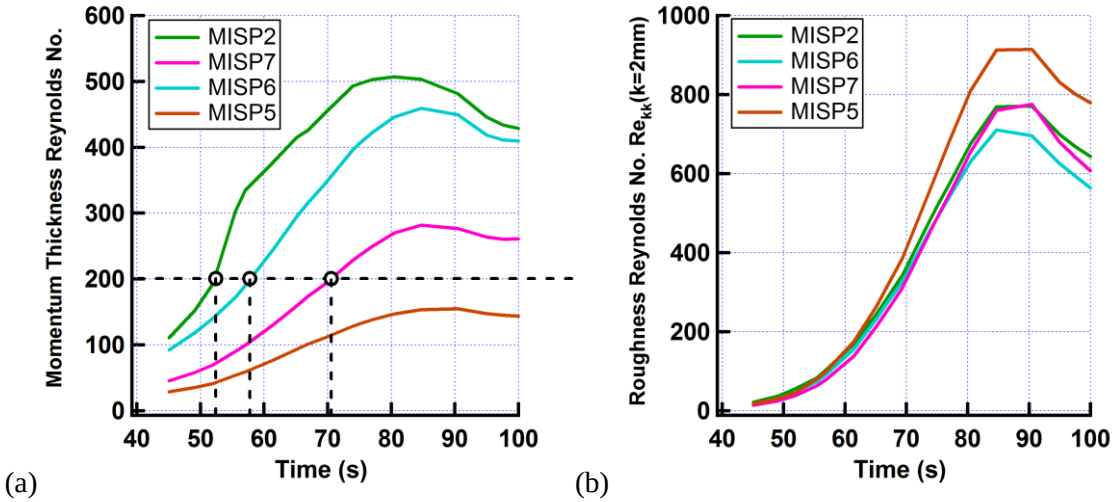

(a) (b)

Figure 8 (a) Re_θ and (b) Re_{kk} (with k=2 mm) traces from laminar CFD computations. MISP 2 and 3 have identical Re_θ and Re_{kk} .

The prediction of boundary layer transition time for design is generally made using a critical Reynolds number based correlation such as the momentum thickness Reynolds number, Re_θ >200 [Ref. 22] for smooth surfaces or one of the roughness based transition criteria for Re_{kk} [Ref. 23], where k is the characteristic roughness height. Figure 8 shows time variation of Re_θ and Re_{kk} based on laminar CFD computations at four leeside plugs. It is seen that Re_θ >200 predicts an earlier transition for MISP2, 3 and 6, but a later transition for MISP7 relative to observations in

flight data. The Re_θ correlation predicts a slower progression of the transition front forward. The Re_θ >200 criteria, therefore, is not conservative. The transition times are summarized in Table 5. The roughness based Re_{kk} correlation, however, shows a rapid progression of transition front from MISP2 to MISP7 as observed in the flight data. An assumption of a 2 mm isolated roughness height, measured in post-test arc jet samples, is made.[12] The critical Re_{kk} for transition depends on whether it is caused by isolated roughness (critical value ~600) or distributed roughness (critical value ~250). No roughness Re_{kk} criteria exists for a situation where the boundary layer is repeatedly disturbed by a finite number of discrete roughness elements, as it is expected to occur is flight due to protruding RTV filler between tiles and around MISP plugs. Figure 8 (b) shows that for an isolated roughness element (~2 mm), all four MISP plugs on the leeside have very similar Re_{kk} values and will likely experience transition simultaneously. These observations suggest that surface roughness may be the cause of transition.

Table 5: Boundary layer transition times from MISP data compared to predictions from Re_θ >200

Plug	Flight Transition Time (sec)	Predicted Transition Time with Re_θ>200 (sec)
MISP3	63	52
MISP2	64	52
MISP6	65	57
MISP7	65	70
MISP5	73	No transition

COMPARISONS OF MODEL PREDICTIONS WITH FLIGHT DATA

Comparisons of CFD pressure with MEADS data

Figure 9 shows comparisons of DPLR and LAURA CFD predictions of surface pressure with MEADS data. The comparisons look excellent which is perhaps not surprising since the BET that is used here is generated using MEADS data and a CFD model. The CFD model is used to estimate freestream parameters from the surface pressure. The comparisons in Fig. 9 therefore serve as a verification of trajectory reconstruction and CFD runs. The agreement between the CFD and MEADS data is within 2%.

Comparisons of Model Predictions with MISP Thermocouple Data

Figure 10 shows initial comparisons of as received data with model predictions using the BET. It is important to emphasize that boundary layer transition times extracted from the flight data (shown in Table 5) are used to switch the imposed CFD aerothermal environments from laminar to turbulent heating over a period of a quarter-second. The discussion in this section is divided into three parts: stagnation region (MISP 1&4), apex region (MISP5 & 7), and the leeside region (MISP2,3,&6).

Stagnation Region (MISP1 & 4). In both plugs the in-depth peak temperatures at the top thermocouple is under predicted by about ~90 C. The under prediction of the peak temperature could be due to a variety of reasons; the most likely cause being a lower prediction of stagnation point heating. A complete sensitivity analysis is underway to detect primary factors that could explain this discrepancy. It is unlikely to be due to errors in the flight trajectory used for the CFD

since the predictions of pressure versus time shows an excellent match with measurements obtained from MEADS instrumentation as shown in Fig. 9. Other causes such as surface recession, surface emissivity, nonequilibrium surface chemistry, high temperature thermal properties of char, and presence of radiative heating are being explored. It is worth noting that an under prediction of stagnation point heating is also seen when comparisons are made with wind tunnel data, especially at turbulent conditions.[3] In MSL TPS sizing, a stagnation point heating margin of about 50% was implemented to account for this under prediction (see Table 1). The under prediction of the wind tunnel data has, however, been hypothesized to be due to tunnel related causes such as freestream turbulence or particle impact, etc. In light of the comparisons with flight data, a re-assessment of our ability to predict stagnation point aeroheating in high Reynolds number flow must be made. It is also seen in Fig. 10 that the prediction of in-depth temperatures is generally better as a fraction of the maximum temperature at that depth. A better comparison in-depth in the relevant time period is because the temperature rise deeper in the material is mostly dependent on the initial portion of the heat pulse, which is generally found to compare well between model and data.

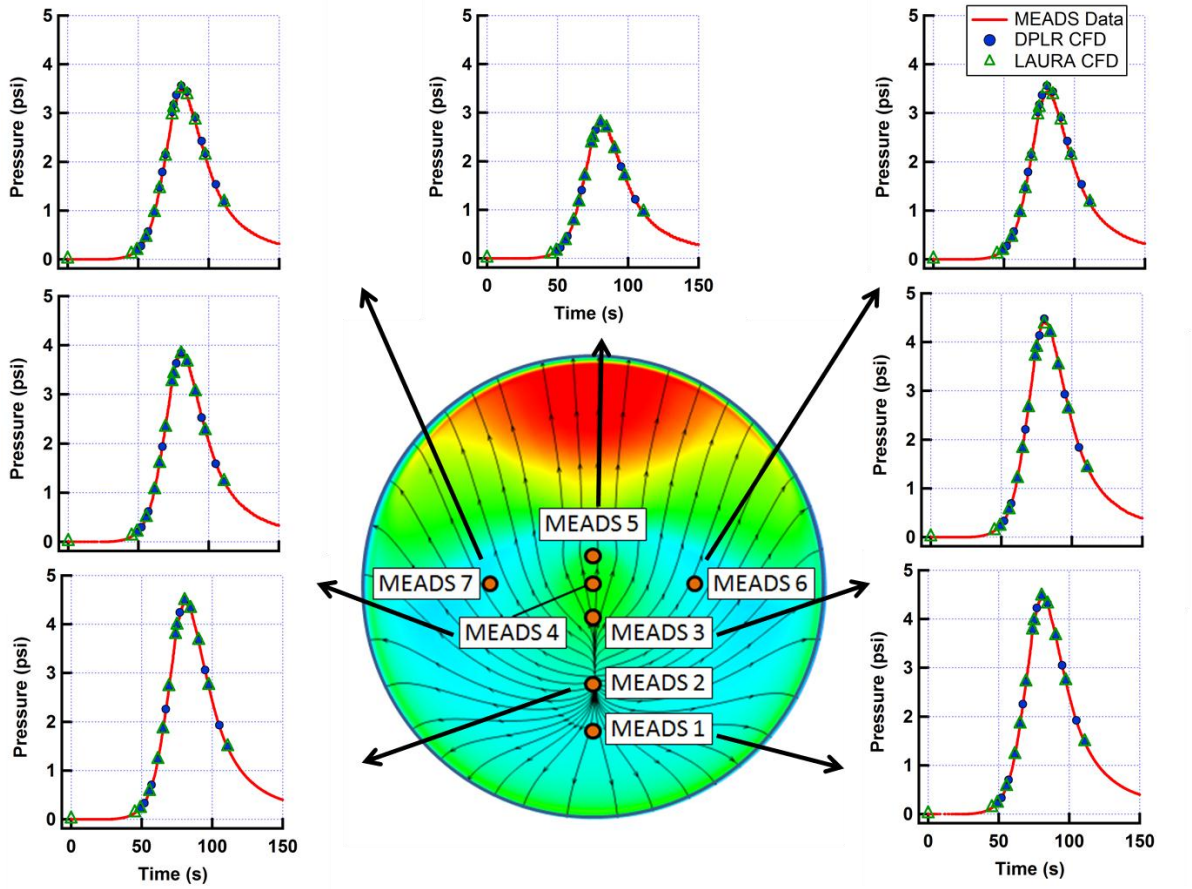

Figure 9 Comparisons of LAURA and DPLR predictions with MEADS pressure measurements

Apex Region (MISP5 & 7). The laminar heating is highest in the apex region near MISP5 (see Fig. 5(a)) where the flow turns around a relatively low radius of curvature surface. On MISP5 & 7, similar to the stagnation region, the peak temperatures are under predicted by the models. Some causes for this discrepancy could be similar to those discussed for stagnation region heating under prediction. At MISP5 the peak predicted temperature is lower by about ~115 C for the near

surface thermocouple. Surprisingly, the highest MISP temperature measured is at MISP7 which has neither the highest laminar nor the highest turbulent heating according to model predictions, although, the vicinity of MISP7 has a large variation of heat flux due to changing radius of curvature of the surface. An evaluation of heating profiles near the apex region will be made to address this discrepancy.

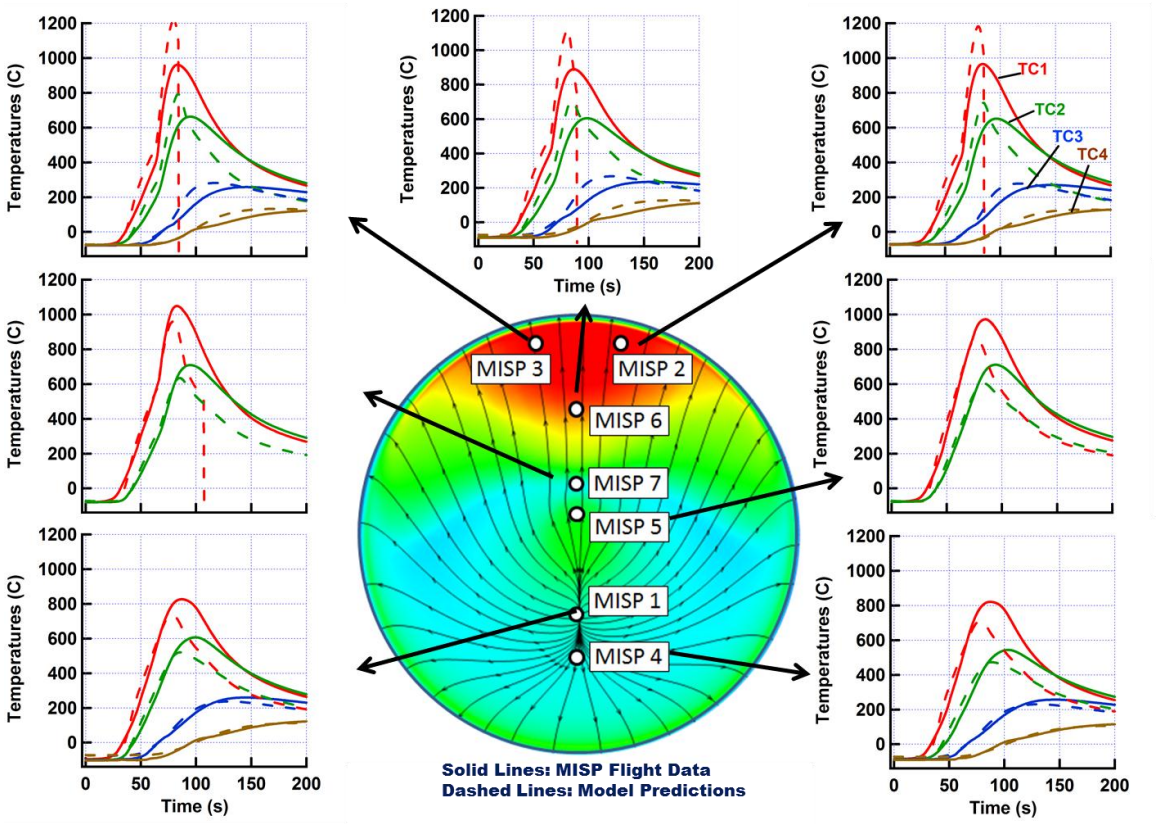

Figure 10 MISP thermocouple data obtained during MSL entry compared with nominal (unmargined) model predictions. TC1, TC2, TC3, and TC4 are thermocouples traces at depths shown in Table 2.

*Leeside Region (MISP2, 3 & 6).*_The leeside of the vehicle forebody clearly experienced turbulent heating. Initial comparisons of the temperature data shows that, unlike other regions of the heatshield, the predicted peak temperatures are much higher than measurement. In fact, the top thermocouple temperature in model prediction continues to rise until the surface recession front reaches the thermocouple depth, which is nominally 2.54 mm (0.1 inch). In flight, however, the recession front does not reach the top thermocouple as discussed before. Recession and the proximity of the top thermocouple to the ablator surface are critical factors that need to be assessed before reasonable predictions of the top thermocouple temperatures are made. Due to a high temperature gradient between the top thermocouple and the surface, the distance between the two is a critical factor. The sensitivity of temperature predictions on surface recession is considered in the next section.

Recession Sensitivity

Although the top thermocouple is installed nominally at 2.54 mm (0.1 inch) from the unablated surface, recession during entry reduces this distance. This is a critical region through

the ablator thickness as the temperature gradient in the top layer of the ablator can be as high as 300 C/mm during peak heating. The temperature at the top thermocouple is therefore expected to be sensitive to the instantaneous depth of the thermocouple (i.e. recession). In this preliminary assessment we re-ran model predictions with no recession to quantify the bounds of variability in temperature predictions. Figure 11 shows the comparisons when surface recession is turned off. The model predictions are now closer to the MISP temperatures at the leedside plugs (MISP2, 3 & 6). However, the predictions are worse for MISP7 & 5. The level of comparison is minimally affected in the stagnation region since total recession is low in this area. The intent here is to only show the sensitivity to recession, and it is not claimed that TPS recession is non- existent in flight.

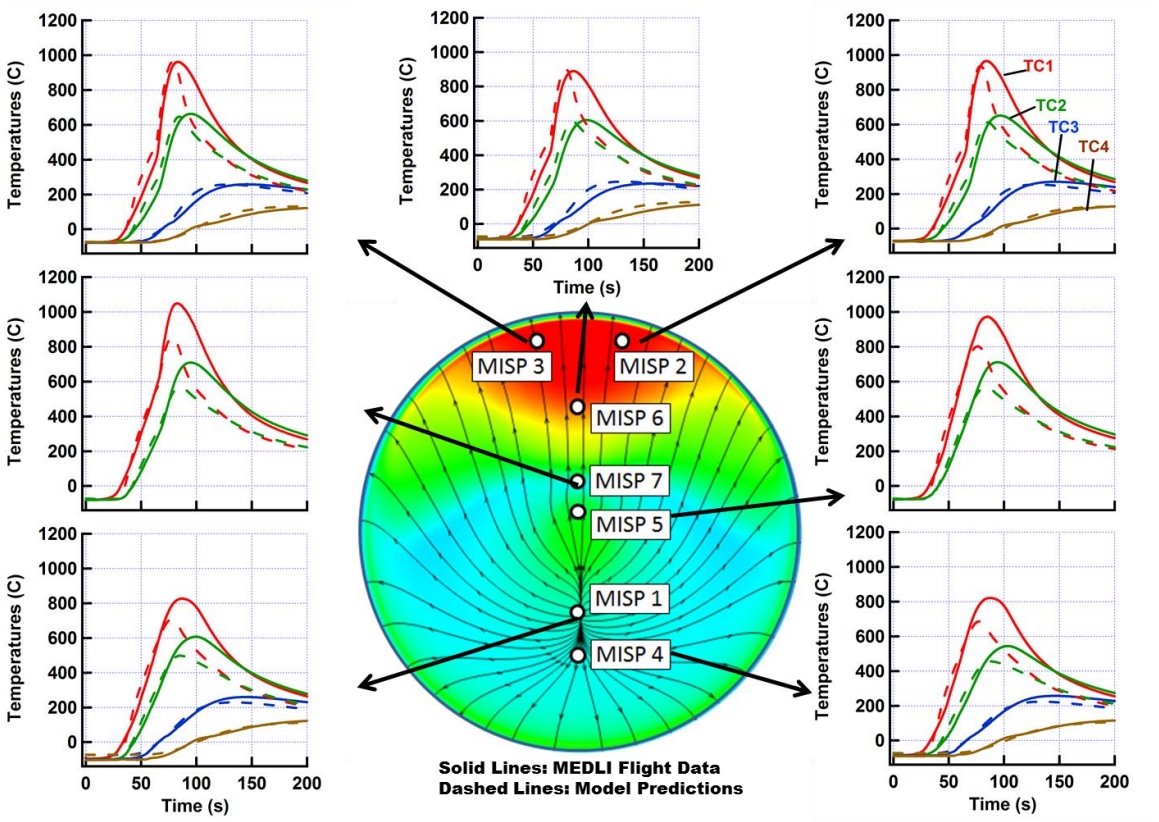

Figure 11 MISP thermocouple data obtained during MSL entry compared with model predictions when surface recession is turned off. TC1, TC2, TC3, and TC4 represent thermocouple traces at depths shown in Table 2.

AEROTHERMAL RECONSTRUCTION

The objective of aerothermal reconstruction is to estimate time-varying surface heating at seven MISP locations during entry. Since the MISP sensors measure in-depth temperatures and not surface heating, a material response model that relates surface aerothermal parameters to in-depth temperatures is needed. FIAT, the material response code discussed earlier, is chosen in an inverse reconstruction process. An inverse reconstruction (IR) attempts to estimate the surface heating by minimizing the difference between the system response model predictions and sensor measurements. An IR methodology has been developed by Mahzari *et al.*[13] specifically for MEDLI post flight analysis. The technique uses a whole time domain approach to estimate time varying heating from in-depth temperature measurements. The technique has been successfully

applied in reconstruction of Mars Pathfinder entry environment based on in-depth thermocouple measurements.[10]

This section presents key aeroheating parameters estimated from the IR technique. It is important to emphasize that since the IR technique uses FIAT material response model for surface heating reconstruction, any approximations, assumptions, and deficiencies in the model and in the properties of charred PICA material will result in an error in the reconstruction. Figure 12 shows reconstructed time-varying surface heating using the IR technique. Table 6 shows peak heating values estimated with and without recession. The surface heating values in Table 6 and Fig. 12 are for a charred ablating surface with pyrolysis gas blowing. These heating values cannot be directly compared to CFD heat flux predictions unless the modeling includes gas-ablative-surface interactions and pyrolysis gas blowing. The same is true for any comparisons made with wind tunnel measurements on non-ablating test articles.

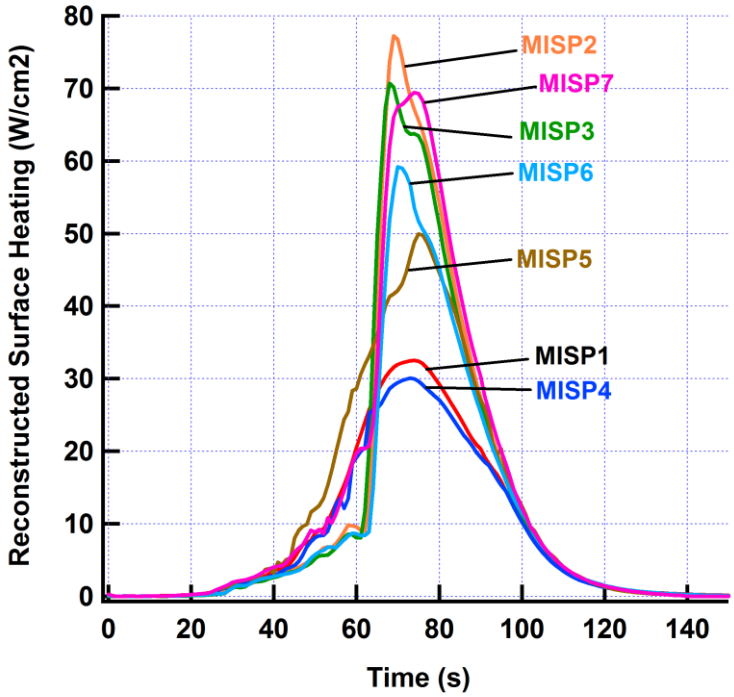

Figure 12. Reconstructed time-varying surface heating using IR assuming no recession. The surface heating is for the pyrolyzing PICA ablator with equilibrium conditions.

UNCERTAINTY ASSESSMENT

The flight data, modeling results, and aerothermal reconstruction shown here have uncertainties associated with them. These uncertainties are caused by instrumentation limitations, inadequate model fidelity, and deficiencies in numerical techniques. An error budget for MISP instrumentation is being developed.[12] An assessment of various instrumentation errors and sources of uncertainty are based on various data sources from manufacturing, installation, laboratory tests, arc jet tests, simulations, and literature review. An initial itemized quantification and substantiation of various errors are provided in Ref. 12. For MISP thermocouples, accuracy of EMF output, impact of thermal gradients, chemical interactions, thermal lag and perturbation, electrical shunting, bead location, etc. have been considered. Additional errors arising due to perturbation or interference caused by the instrumentation and plug integration into the TPS, are

also being evaluated. Some of these errors and uncertainties are being estimated using controlled tests in arc jet facilities in flight relevant environment.

Table 6. Reconstructed surface heating (W/cm^2) of charring and pyrolyzing PICA ablator

	MISP1	MISP2	MISP3	MISP4	MISP5	MISP6	MISP7
With Nominal Recession	28.0	63.4	57.5	26.0	37.0	50.7	54.5
Without Recession	32.5	77.2	70.7	30.0	49.9	59.2	69.4
Change	4.5	13.8	13.2	4.0	12.9	8.5	14.9

The modeling and inverse reconstruction also have uncertainty that arise due to insufficient model fidelity, numerical errors, and the use of simplifying assumptions. For example, unknown recession causes a significant variation of about 5-15 W/cm^2 in reconstructed surface heating as shown in Table 6. An uncertainty in reconstructed surface heating also occurs due to uncertainties in near surface thermocouple depth measurements, surface emissivity, and thermal conductivity of charred and virgin PICA among others, as shown in Fig. 13. Surface emissivity could be uncertain due to possible silica melt coverage over the ablator surface, which has been observed in arc jet tests at low heat flux conditions. The high temperature properties, like thermal conductivity, are also somewhat uncertain due to difficulty in making controlled high temperature material property measurements. A comprehensive sensitivity and uncertainty analysis is underway to quantify these uncertainties and their impact, and will be presented in future.

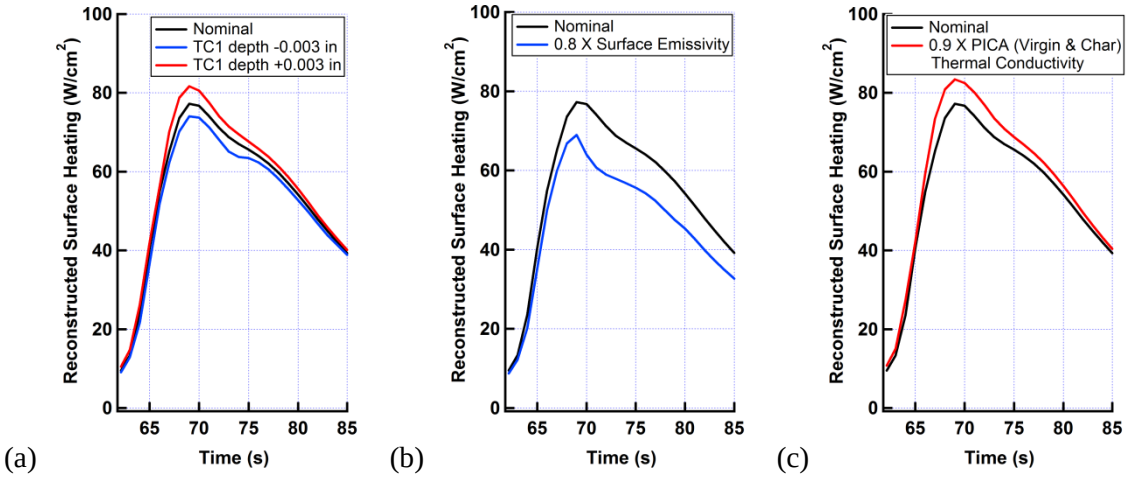

Figure 13. Sensitivity of reconstructed surface heating to variation/errors in (a) near surface thermocouple depth, (b) surface emissivity, and (c) PICA (virgin and char) thermal conductivity

CONCLUSIONS

An initial assessment of the MEDLI-MISP data using the current BET is presented. The initial assessment of MISP temperature data suggests a lower than predicted TPS recession and a roughness induced boundary layer transition to turbulence on the leeside forebody of the vehicle. A comparison of MISP temperature data with model predictions shows an underprediction of temperatures in the stagnation and the apex regions, and an overprediction in the leeside region.

The agreement on the leeside improves significantly if the recession is suppressed. An inverse reconstruction technique is used to estimate time-varying surface heating of the pyrolyzing and charring PICA ablator. A surface heating value as high as 77.2 W/cm^2 is found on the leeside region when no recession is allowed. The reconstructed values have uncertainty due to model assumptions, thermocouple depth uncertainty, surface emissivity, material property uncertainty, etc. A comprehensive sensitivity analysis is being conducted to explain the remaining differences between model predictions and flight data.

ACKNOWLEDGEMENTS

We would like to thank MEDLI and Hypersonics Project Management, especially Alan Little, Michelle Munk, Jim Pittman, and Michael Wright for their support and advocacy for this work. Special thanks are due to Chris Kuhl and Ron Verhappen. We would like to acknowledge the assistance of MSL project staff at Jet Propulsion Laboratory and other NASA centers. This work would not be possible without the help and support from NASA Ames TPS Sensor group led by Ed Martinez, and the personnel at the NASA Ames Arc Jet Complex. Technical input from Dan Reda, Y.K. Chen and Frank Milos are also acknowledged. Portions of this work are conducted under NASA contract NNA10DE12C to ERC, Incorporated and a NASA grant NNX12AF94A (Principal Investigator: Prof. Robert Braun) to Georgia Institute of Technology.

REFERENCES

[1]A. Steltzner, "Mars Science Laboratory Entry Descent Landing System Overview," AAS 2013-236, Feb. 2013.

[2]R.A.S. Beck, et al., "Development of the Mars Science Laboratory Heatshield Thermal Protection System," AIAA Paper 2009-4229, June 2009.

[3]K.T. Edquist, A. A. Dyakonov, M. J. Wright, and C.Y. Tang, "Aerothermodynamic Design of the Mars Science Laboratory Heatshield," AIAA Paper No. 2009-4075, June 2009.

[4]M.J. Wright, et. al, "Sizing and Margins Assessment of the Mars Science Laboratory Aeroshell Thermal Protection System" AIAA Paper No. 2009-4231, June 2009.

[5]M. Gazarik, et al. "Overview of the MEDLI Project," IEEE Paper 2008-1510, March 2008.

[6]A. Little, et al., "Mars Science Laboratory (MSL) Entry, Descent, and Landing Instrumentation (MEDLI): hardware Performance and Data Reconstrcution," AAS 2013-078, Feb. 2013.

[7]D. Bose, M.J. Wright, and G.E. Palmer, "Uncertainty Analysis of Laminar Aeroheating Predictions for Mars Entries," Journal of Thermophysics and Heat Transfer, Vol. 20, No. 4, Oct-Dec 2006, pp. 652-662.

[8]K.T. Edquist, M.J. Wright, and G.A. Allen, "Viking Afterbody Heating Computations and Comparisons to Flight Data," AIAA Paper 2006-386, Jan 2006.

[9]Milos, F., Y-K. Chen, W. Congdon, and J. Thornton, "Mars Pathfinder Entry Temperature Data, Aerothermal Heating, and Heatshield Material Response," *Journal of Spacecraft and Rockets*, Vol. 36, No. 3, 1999, pp. 380-391.

[10]M. Mahzari, R.D. Braun, and T.R. White, "Reconstruction of Mars Pathfinder Aerothermal Heating and Heatshield Material Response Using Inverse Methods," AIAA-Paper 2012-2872, Jun 2012.

[11]C.D. Karlgaard, P. Kutty, M. Schoenenberger, J. Schidner, and M. Munk, "Mars Entry Atmospheric Data System Trajectory Reconstruction Algorithms and Flight Results," AIAA Paper 2013-0028, Grapevine, TX, Jan 2013.

[12]D. Bose, T. White, J.A. Santos, J. Feldman, M. Mahzari, M. Olson, and B. Laub, "Initial Assessment of Mars Science Laboratory Heatshield Instrumentation and Flight Data," AIAA Paper 2013-0908, Grapevine, TX, Jan 2013.

[13]M. Mahzari, R.D. Braun, T. White, and D. Bose, , "Preliminary Analysis of the Mars Science Laboratory's Entry Aerothermodynamic Environment and Thermal Protection System Performance," AIAA Paper 2013-0185, Jan 2013.
[14]M. Munk, A. Little, C. Kuhl, D. Bose, and J. Santos, "The Mars Science Laboratory (MSL) Entry, Decent and Landing Instrumentation (MEDLI) Hardware." AAS 13-310, 23rd AAS/AIAA Spaceflight Mechanics Meeting, Kauai, HI, February 10-14, 2013.
[15]S. Gorbunov et al. "Thermal Protection System Ablation Sensor," US Patent 8,069,001 B1, Nov. 29, 2011.
[16]M. J. Wright, G. V. Candler, and D. Bose, , "Data-Parallel Line Relaxation Method of the Navier-Stokes Equations," *AIAA Journal*, Vol. 36, No. 9, 1998, pp., 1603-1609.
[17]P.A. Gnoffo, "An Upwind Biased, Point-Implicit Relaxation Algorithm for Viscous, Compressible Perfect-Gas Flows," NASA TP-2953, 1990.
[18]F.S. Milos and Y.K. Chen, "Comprehensive Model for Multicomponent Ablation Thermochemistry," AIAA-97-0141, Jan 1997.
[19]F.S. Milos and Y.K. Chen, "Ablation and Thermal Response Property Model Validation for Phenolic Impregnated Carbon Ablator," *Journal of Spacecraft and Rockets*, Vol. 47, No. 5, 2010, pp. 786-805.
[20]R.A. Mitcheltree and P.A. Gnoffo, "Wake Flow About a MESUR Mars Entry Vehicle," AIAA 94-1958, June 1994.
[21]F. Milos, Y-K. Chen, and T. Gokcen, "Non-Equilibrium Ablation of Phenolic Impregnated Carbon Ablator," AIAA Paper 2010-981, Jan 2010.
[22]B.R. Hollis and A.S. Collier, "Turbulent Aeroheating Testing of Mars Science Laboratory Entry Vehicle," *Journal of Spacecraft and Rockets*, Vol. 45, No. 3, May-Jun. 2008, pp. 417-427.
[23]D.C. Reda, M.C. Wilder, and D.K. Prabhu, "Transition Experiments on Blunt Bodies with Isolated Roughness Elements in Hypersonic Flight," *Journal of Spacecraft and Rockets*, Vol. 47, No. 5, Sept.-Oct. 2010, pp. 828-835.